Computer Science Journal of Moldova, vol.**22**, no.2(65), 2014

Characterization and pattern recognition of color images of dermatological ulcers: a pilot study*

Invited Article

Lucas C. Pereyra, Sílvio M. Pereira, Juliana P. Souza, Marco A. C. Frade, Rangaraj M. Rangayyan, Paulo M. Azevedo-Marques

Abstract

We present color image processing methods for the characterization of images of dermatological lesions for the purpose of content-based image retrieval (CBIR) and computer-aided diagnosis. The intended application is to segment the images and perform classification and analysis of the tissue composition of skin lesions or ulcers, in terms of granulation (red), fibrin (yellow), necrotic (black), callous (white), and mixed tissue composition. The images were analyzed and classified by an expert dermatologist following the red-yellow-black-white model. Automatic segmentation was performed by means of clustering using Gaussian mixture modeling, and its performance was evaluated by deriving the Jaccard coefficient between the automatically and manually segmented images. Statistical texture features were derived from cooccurrence matrices of RGB, HSI, $L^*a^*b^*$, and $L^*u^*v^*$ color components. A retrieval engine was implemented using the k-nearest-neighbor classifier and the Euclidean, Manhattan, and Chebyshev distance metrics. Classification was performed by

*This work was partially supported by The National Council for Scientific and Technological Development (CNPq) — grants 472508/2010-5, 304225/2010-0, and 573714/2008-8 (INCT/INCoD), and the Natural Sciences and Engineering Research Council of Canada.

means of a metaclassifier using logistic regression. The average Jaccard coefficient after the segmentation step between the automatically and manually segmented images was 0.560, with a standard deviation of 0.220. The performance in CBIR was measured in terms of precision of retrieval, with average values of up to 0.617 obtained with the Chebyshev distance. The metaclassifier yielded an average area under the receiver operating characteristic curve of 0.772.

Keywords: Color image processing, color medical images, color texture, content-based image retrieval, computer-aided diagnosis, image segmentation, dermatological ulcers, tissue composition analysis.

1 Introduction

1.1 Computer-Aided Analysis of Medical Images

Recent developments in information and communication technologies have led to the creation and use of huge archives of multimedia data in diverse application areas, such as medical imaging, remote sensing, entertainment, education, and online information services. Traditional database management systems were designed to organize alphanumeric data into interrelated collections so that information storage and retrieval could be performed conveniently and efficiently. However, such methods are not well suited for the organization, management, and efficient use of multimedia information [1]. In many practical applications, the retrieval of a specific image from a database of images could be an important task [2]. Several search engines are available for searching and retrieval of textual and pictorial information [2–5]. However, general-purpose tools for searching and retrieval of data are not suitable for specialized medical applications. For this reason, specific methods and systems for the characterization, searching, and retrieval of image-based data are being developed for particular medical imaging applications [6, 7], such as mammography [8–11], chest and other radiographic imaging [12,13], dermatological lesions [14–17], and pathology [18].

The traditional approach of indexing images using manual notes (textual annotation) is slow, labor-intensive, and expensive. In addition, textual annotations cannot effectively encode all of the information available in a given image. Furthermore, image features based on huge amounts of pixel data, complex concepts of application-specific patterns, and domain-specific notions may not lend themselves to easy or efficient textual description. Thus, there is a need to develop advanced methods of image processing, feature extraction, quantitative representation, and pattern recognition for effective and efficient indexing and retrieval of images based on their content.

Content-based image retrieval (CBIR) refers to searching, selection, and retrieval of images from a database that are similar to a query image, using measures of information derived from the images themselves, rather than relying on the accompanying text or annotation [6, 19]. To facilitate CBIR, the contents of the images need to be characterized by quantitative features. The features of the query image may then be compared with the features of each image in the database, and images having high similarity with respect to the computed features of the query image may be retrieved and displayed [19]. CBIR of medical images is a useful tool, and could provide physicians with assistance in the form of a display of relevant past cases with proven pathology, along with the associated clinical, diagnostic, and other information [19].

The potential use of automated image categorization techniques to assist physicians in diagnosis led to intense research in the field of medical image processing classification [19–21]. This approach usually consists of mapping images into predefined classes and involves the steps of representation (description of image content by feature extraction), adaptation (selection of the most representative subset of features to classify information) and, generalization (the training and evaluation of a classifier) [19, 21, 22].

The same steps mentioned above may also be used to assist in clinical decision making and lead towards computer-aided diagnosis (CAD) [19, 21, 23]. The medical domain has specific requirements (high sensitivity and low false-negative as well as false-positive rates) and errors in detection are extremely costly, making the development of a

computerized scheme to aid diagnosis with broad application in clinical practice a challenge [19, 20].

1.2 Analysis of Dermatological Ulcers

Ulcers on the lower limbs can be described as the irregular loss of the epidermis, also possibly involving the dermis and subcutaneous tissue. They affect approximately 1% of the population, causing considerable morbidity [24]. This condition is usually ascribed to a deficiency in blood flow due to venous or arterial insufficiency, and can be caused by ailments such as diabetes mellitus, autoimmune diseases, and local infections. The ulceration may be referred to as a wound, lesion, or ulcer, and medical professionals in dermatology base the diagnosis of skin lesions mainly on visual assessment of pathological regions and the evaluation of macroscopic features. This fact indicates that correct diagnosis is highly dependent on the observer's experience and visual perception [16, 25]. Accurate wound assessment is a critical task in patient care and important for the reduction of costs of care in hospitals. However, this task still relies on manual procedures and tedious practices. Wound shape is measured with rulers and tracing paper, or rarely with alginate castings and serum injection.

Healing is a complex cascade of cellular events operating to reconstruct damaged tissues, and also an individual process that exhibits considerable interpatient variability. As the different tissues may overlap and be difficult to distinguish, wound assessment is not straightforward. The lack of quantitative data affects the coordination of healthcare staff and hinders clinical studies focused on healing. Digital cameras, though now widespread in clinical centers, are used mostly for basic patient data recording and not image processing [17].

The appearance of a wound, lesion, or ulcer provides important clues that can help with the diagnosis, determination of severity, and the prognosis of healing [26, 27]. Chronic skin lesions, wounds, or ulcers typically have a nonuniform mixture of red granulation, yellow fibrin (slough), and black necrotic scar tissue. Thus, a red-yellow-black (RYK) model is used by physicians in a descriptive manner [15, 17, 26–29]. In clinical assessment, the category of callous lesions,

composed predominantly of white tissue, is also used. Therefore, an extended version of the RYK model, including white (RYKW) one, may be of interest. The quantification of texture and color distribution in lesions by image processing techniques could assist in the analysis of the dynamics of the pathological process, as well as of healing and response to treatment [17, 27, 29, 30]. Such quantitative analysis, in turn, can be used to design optimized and personalized treatment protocols for each patient.

In a clinical scenario, the possibility of retrieving images from an established database that are similar to the case on hand, based on digital image processing techniques that characterize the color composition of lesions, could facilitate understanding how dermatological lesions are classified and assist in arriving at a diagnostic or therapeutic decision. In this context, efficient systems for content-based indexing and retrieval [6, 27, 31], as well as methods to perform classification of wounds based on the types of tissue present in the wound are useful and could help health professionals assess lesions for any of the aforementioned purposes.

Celebi et al. [32] described a system to retrieve skin lesion images based on shape similarity, using a database with 184 skin ulceration images in cases of melanoma. The agreement between computer assessment and human perception was indicated by values of up to 0.73, when similarity functions were optimized using a genetic algorithm. Dorileo et al. [14] proposed a CBIR system for images of dermatologic ulcers. Features based on histogram and multispectral cooccurrence matrices were used for image retrieval. Performance was evaluated based on precision values with a database of 215 images. The best precision result was 70% for mixed tissue composition images. Rahman et al. [33] presented a CBIR system for dermatoscopic images. Image processing, segmentation, feature extraction (color and texture), and similarity matching were performed on a database comprising 358 images of pigmented skin lesions in three categories (benign, dysplastic nevi and, melanoma). The analysis of precision curves displayed the ability of their system to retrieve visually similar lesions with an average precision value of 60%.

The variability and inhomogeneity of tissues makes color analysis for tissue classification innefective if the methods are applied directly on the pixels with simple thresholds on separate color components. Spatial continuity needs to be incorporated, which suggests that the classification process should be guided by a segmentation step [34]. Color histograms are commonly utilized as descriptors for statistical data analysis [35], and the use of hybrid tissue classes and limiting classification to a reduced number of tissue types have also been reported, with an average accuracy of 88.7% using a k-nearest-neighbor (kNN) classifier [29].

In previous related work, we evaluated the performance of different distance metrics for CBIR of dermatological images [31]. A database of 172 manually segmented images was used. CBIR using a kNN classifier and the Euclidean, Manhattan, Chebyshev, cosine, and correlation distances was performed. The best results were obtained with the cosine and correlation distances, with average precision of 75%. We also performed automatic segmentation using methods of color clustering and mathematical morphology [36]. The same database of 172 images was used. The average Jaccard coefficient between automatically and manually segmented regions was 0.56, with a standard deviation of 0.22.

The present work, which is an expanded and updated version of recent conference presentations [31, 36], focuses on quantitative assessment of color components in images of ulcers on the lower limbs. We present techniques to perform analysis of color components, texture analysis, and automatic segmentation. Results are presented and discussed in the context of CBIR and computer-aided diagnosis CAD [15–17, 27, 28, 30, 31, 36].

2 Materials and Methods

2.1 Database of Images

A database consisting of 172 dermatologic images has been prepared to date, based on 63 consecutive medical examinations of outpatients

at the University Medical Center at the Ribeirão Preto Medical School of the University of São Paulo, Brazil. Approval was obtained from the Medical Center Ethics Committee for this research. Images were obtained based on a specific protocol that was determined after initial tests [14]. All images were obtained with the same digital camera (Canon EOS 5D0, 2 Megapixels), a 50-mm macro lens, and a polarization filter; see Figure 1 for examples of images of various types of ulcers. The typical size of the color images is 1747×1165 pixels with 24 bits/pixel. The tissue composition of each lesion was classified independently by an expert dermatologist (MACF), based on the color composition, as granulation (red), fibrin (yellow), and mixed tissue. The 172 images in the database include 51 images of lesions predominantly composed of granulation, 31 images of fibrin, three images of callous, three images of necrotic, and 84 images of mixed tissue. The dermatologist also drew the boundaries of the lesions.

A blue cloth was used to create a background in a color not expected within the ulcer or on the part of the body being imaged, as can be seen in Figure 1, parts (c) and (d). Color patches and rulers were included in the images (see Figure 1) to facilitate color normalization and calibration of the images. A suite of color image processing techniques, pattern analysis, classification methods, and graphical user interfaces (GUIs) is being developed to facilitate image analysis, CAD, and CBIR [14, 27, 28, 31, 37].

2.2 Automatic Segmentation of the Ulcer Region

A color clustering process using an expectation maximization (EM) procedure based on a multivariate Gaussian mixture model [37, 38] was applied to each hue-saturation (HS) histogram [39]. The EM algorithm implemented in the present work is an iterative method for finding maximum-likelihood or maximum-a-posteriori (MAP) estimates of parameters in statistical models. The EM iteration alternates between performing an expectation (E) step, which creates a function for the expectation of the log-likelihood evaluated using the current estimate for the parameters, and a maximization (M) step, which computes param-

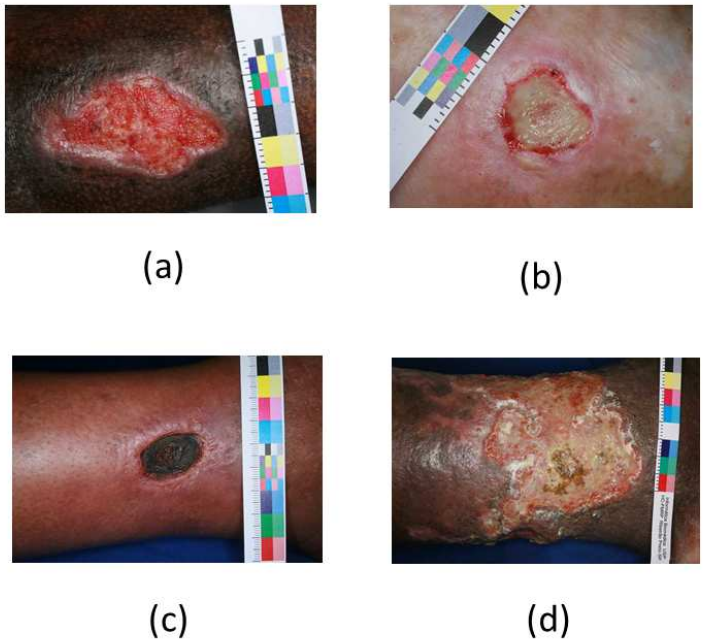

Figure 1. Examples of images of various types of ulcers: (a) predominantly granulation, (b) predominantly fibrin, (c) predominantly necrotic tissue, and (d) mixed tissue composition.

eters maximizing the expected log-likelihood found in the E step. The initialization assumes that the whole set of values in the HS histogram can be clustered into just one Gaussian distribution. This hypothesis is tested based on the values of the mean and standard deviation of a sample of 1,000 values obtained randomly from the HS histogram, considering an estimation error of 0.0001%. If the hypothesis is not true, that is, if the Gaussian adjustment error for the sample is greater than the specified error, a new iteration is performed, assuming the mixture of two Gaussians. The procedure is iterated until every pixel in the sample belongs to a cluster, or the number of iterations reaches a specified limit (100 cycles). The clustering procedure was developed using the Waikato Environment for Knowledge Analysis (WEKA) [41].

After color clustering, the set of clusters representing the tissue composition of the ulcer was manually selected. A GUI was implemented using the Java programming language and the NetBeans[1] environment to facilitate cluster selection. To fill any residual gap, a method based on mathematic morphology and automatic delineation of the convex hull was implemented using ImageJ plugins and applied to determine the final lesion area. The convex hull is defined as the smallest convex polygon that encompasses a set of points [42]. Figure 2 shows an example of an image of an ulcer and the corresponding result of segmentation.

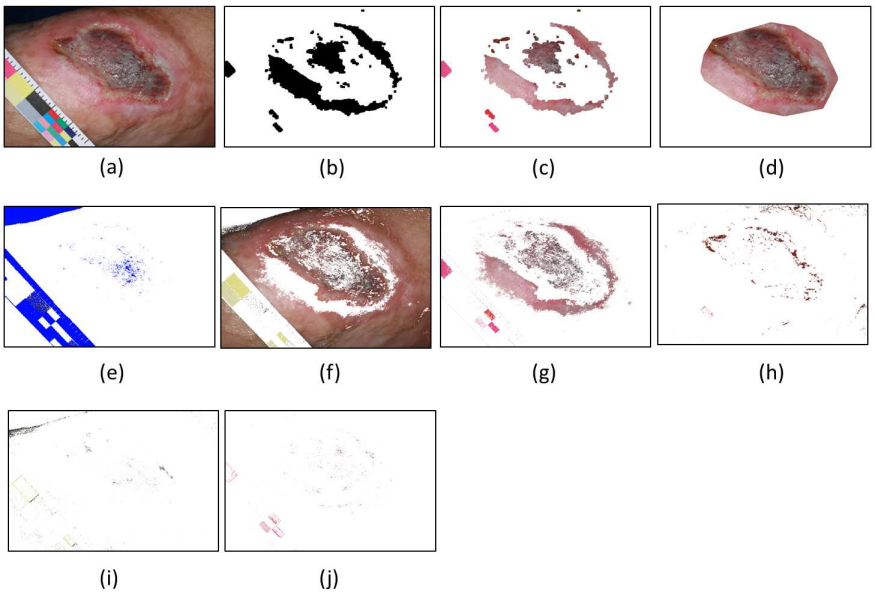

Figure 2. Example of ulcer segmentation. The clustering process resulted in six clusters (e) to (j). (a) shows the original image, (b) the segmentation mask generated by manual cluster selection followed by application of mathematic morphology operations, (c) is the partial segmented area, and (d) is the final lesion area after automatic delineation of the convex hull.

[1] `https://netbeans.org/`. Accessed on 01/04/2014.

2.3 Feature Extraction and Indexing of Images

Feature extraction was based on the automatically segmented regions. For each region representing a lesion, in addition to the basic RGB color components, six images were generated. According to the HSI representation, an image (I) was generated based on the hue (H) component and another was generated based on the saturation (S) component [39]:

$$I = \frac{R+G+B}{3},$$

$$S = 1 - \left(\frac{3}{(R+G+B)}\right) * a,$$

$$where \quad a \quad is \quad the \quad minimum \quad of \quad R, \quad G, \quad and \quad B,$$

$$H = \cos^{-1} \frac{(0.5*(R-G)+(R-B))}{\left((R-G)^2+(R-B)(G-B)\right)^{0.5}}.$$

The next color representations are based on the CIE XYZ color space. The conversion from RGB to XYZ is performed as follows [40]:

$$\begin{matrix}[R] \\ [G] = \\ [B]\end{matrix} \begin{matrix}[3.240479 & -1.537150 & -0.498535] \\ [-0.969256 & 1.875992 & 0.041556] \\ [0.055648 & -0.204043 & 1.057311]\end{matrix} \begin{matrix}[X] \\ * [Y] \\ [Z],\end{matrix}$$

$$x = \frac{X}{(X+Y+Z)},$$

$$y = \frac{Y}{(X+Y+Z)}.$$

According to the L*u*v* color representation, an image was generated based on the u* component and another was generated based on the v* component:

$$u' = \frac{2x}{(6y-x+1.5)},$$

$$v' = \frac{4.5y}{(6y-x+1.5)},$$

$$L^* \begin{cases} 116\left(\frac{Y}{Y_n}\right)^{\frac{1}{3}} - 16 & if \quad \frac{Y}{Y_n} > 0.008856, \\ 903.3\left(\frac{Y}{Y_n}\right) & if \quad \frac{Y}{Y_n} \leq 0.008856, \end{cases}$$

$$u* = 13\,(L^*)\left(u' - u'_n\right),$$

$$v* = 13\,(L^*)\left(v' - v'_n\right).$$

Similarly, according to the L*a*b* color representation, an image was generated based on the a* component and another was generated based on the b* component:

$$L^* \begin{cases} 116\left(\frac{Y}{Y_n}\right)^{\frac{1}{3}} - 16 & if \quad \frac{Y}{Y_n} > 0.008856, \\ 903.3\left(\frac{Y}{Y_n}\right) & if \quad \frac{Y}{Y_n} \leq 0.008856, \end{cases}$$

$$a* = 500 * (f\,(X/X_n) - f\,(Y/Y_n)),$$

$$b* = 200 * (f\,(Y/Y_n) - f\,(Z/Z_n)),$$

$$where \quad f\,(t) = \begin{cases} t^{\frac{1}{3}} & if \quad t \leq 0.008856, \\ 7.787 * t + 16/116 & if \quad t \leq 0.008856. \end{cases}$$

Values of the mean, standard deviation, skewness, and kurtosis were computed from the histogram of each of the R, G, B, H, S, u*, v*, a*,

and b* components. In addition, the five most discriminative features of the 14 texture features proposed by Haralick et al. [43] were derived from an averaged cooccurrence matrix (CoM) computed from four CoMs for a distance of one pixel at 0, 45, 90, and 135 degrees. The features are homogeneity, contrast, correlation, entropy, and local homogeneity, as suggested by Conners and Harlow [44], and were computed for each of the R, G, B, H, S, u*, v*, a*, and b* components. Furthermore, the five texture features mentioned above were computed from multispectral or color cooccurrence matrices (CCMs), obtained from the RG, GB, BR, HS, u*v*, and a*b* components, using the method proposed by Arvis et al. [45]. The method is an extension of the method of Haralick et al. [43], and was developed for application to color images to take into account the correlation existing between the color components, as shown in Figure 3. Thus, a total of 111 features were extracted from the R, G, B, H, S, u*, v*, a*, and b* components to characterize and index each color image [27, 31, 36].

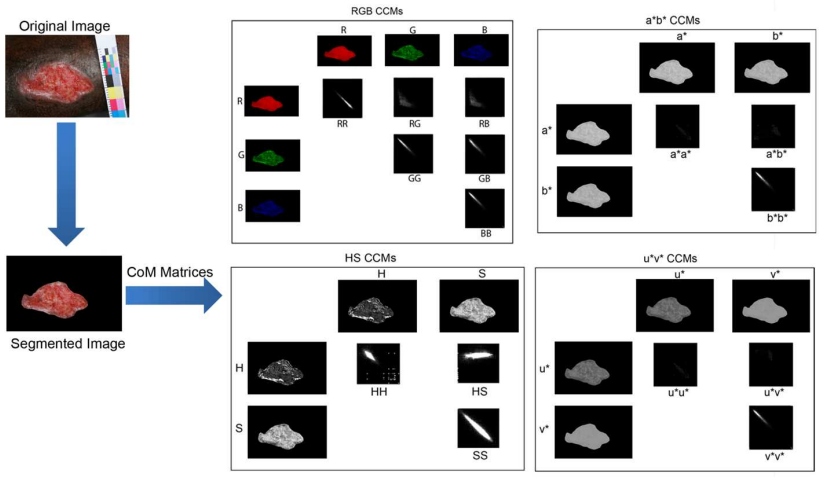

Figure 3. Color cooccurrence matrices (CCMs) obtained from the RGB, HS, u*v*, and a*b* components

2.4 CBIR Experiment

A retrieval engine was developed using the kNN classifier based on the Euclidean, Manhattan, and Chebyshev metrics between the features of the query image and those of each image in the database. The definitions of the metrics are summarized in Table 1. The value of k was varied from 1 to 7 in steps of 2.

Table 1. Distance metrics used in CBIR experiments. In the equations, x is the feature vector of size n of the query image, y the feature vector of size n of an image being considered for retrieval, and d_{xy} is the distance between the two vectors.

Metric Name	Formula
Euclidean	$d_{xy} = \sqrt{\sum_{j=1}^{n} (x_j - y_j)^2}$
Manhattan	$d_{xy} = \sum_{j=1}^{n} \lvert x_j - y_j \rvert$
Chebyshev	$d_{xy} = \max_{j=1}^{n} \{\lvert x_j - y_j \rvert\}$

For every value of k, all images in the database were used, one by one, as the query image. The mean value of the precision of retrieval was computed for each retrieval experiment and for each distance or metric. Precision values for the categories of necrotic and callous ulcers were not computed due to the small numbers of samples available. The precision of retrieval was computed in each experiment as the ratio of the number of relevant images retrieved to the total number of images retrieved. In computing precision, each retrieved image received a binary weight of unity or zero, representing a relevant image or not, respectively; the sum of such scores for all of the retrieved images was then divided by the total numbers of retrieved images. Ten-fold cross validation was the chosen validation method. An image was considered to be relevant when it belonged to the same class as the query image, according to the classification provided independently by the expert dermatologist (MACF). It should be noted that, in a medical application, a clinician would not be interested in the retrieval of a large number of images or cases. A small number of highly relevant

cases, such as 3 or 5 cases, retrieved from a large database along with the related clinical reports, would serve the purpose of assisting in the diagnosis of the current query case. It would not be of interest to retrieve all relevant cases that exist in the database. Thus, in a clinical application, precision would be, in general, more important than other measures of performance of CBIR, such as recall or area under the precision-versus-recall curve.

2.5 Classification Experiment

Classification of images was performed by means of a metaclassifier for handling multiclass datasets with two-class classifiers, as a proxy to the main classifier which it wraps to provide additional data preprocessing before actually training and/or testing of the wrapped classifier. Logistic regression was used as the wrapped classifier. In order to improve the parameters of the estimates and reduce the prediction error, ridge estimators are used to pool highly correlated covariates and reduce overfitting and colinearity [46]. The classification experiment did not include the categories of necrotic and callous ulcers due to the small number of samples available. Validation was also performed using ten-fold cross validation.

3 Results

3.1 Automatic Segmentation of the Ulcer Region

The Gaussian mixture modeling procedure applied to 172 images resulted in a clustering process with the number of clusters varying from 3 to 9, before the manual selection step using the GUI. Processing times for the clustering process ranged from 3 to 5 minutes per image. After cluster selection, the evaluation of the segmentation step indicated an average Jaccard coefficient of 0.56 with a standard deviation of 0.22 between the lesion area obtained computationally and the same lesion region manually delineated by the dermatologist. The Jaccard coefficient (J) is calculated by computing the ratio of the intersection

to the union of the manually and computationally derived regions and has a value range from zero to one, where zero means a total failure of the computational segmentation process and one indicates a perfect segmentation, based on comparison with the manually segmented regions:

$$J(A,B) = \frac{|A \cap B|}{|A \cup B|}.$$

3.2 Analysis of Tissue Composition and Classification of Ulcers

To compare the tissue composition within the lesion regions segmented computationally and manually, a measurement approach was applied based on thresholding of HSI values [31,36,39]. White tissue component was defined as the number of pixels within the lesion with $S \leq 0.2$ and $I \geq 0.75$ (independent of H and with the S and I components normalized to the range 0 to 1); black tissue component was defined as the number of pixels within the lesion with $S \leq 0.2$ and $I \leq 0.2$; red tissue component was defined as the number of pixels within the lesion with $S > 0.2$ and $-30° < H < 30°$ (independent of I); and yellow tissue component was defined as the number of pixels within the lesion with $S > 0.2$ and $30° < H < 90°$. A low average root-mean-squared error (RMSE) [36] of 4% with a standard deviation of 5% was obtained between the RYKW tissue composition vectors of computationally and manually segmented lesions.

Classification results with the metaclassifier using logistic regression were analyzed in terms of correctly classified instances and the average area under the receiver operating characteristic curve (AUC). The ratio between the number of correctly classified instances and the total number of instances was 0.638, and the average AUC value was 0.772. The processing time using all the images from the dataset was less than 3 seconds.

3.3 CBIR

Based on the retrieval experiments performed using different distance measures, precision values were calculated for each image class and an average precision value was derived. The Processing time was less than 1 second for all CBIR experiments. The most significant distance regarding precision values was the Chebyshev distance. For $k = 1$, the average precision was 0.617 (as compared to 0.587 and 0.550 using Manhattan and Euclidean distances, respectively), and for $k = 3$, the average precision was 0.609 (as compared to 0.566 and 0.538 using Manhattan and Euclidean distances, respectively). The rates of precision for values of $k = 5$ and 7 were lower than those previously mentioned, for all of the distances considered in this study. Tables 2 and 3 display the confusion matrices for the kNN procedure with $k = 1$ and 3 and using the Chebyshev distance, respectively.

Table 2. Confusion matrix for the CBIR experiment, using a kNN classifier with $k = 1$ and the Chebyshev distance.

Red	Yellow	Mixed	Retrieved for
31	3	17	Red
3	20	8	Yellow
26	8	50	Mixed

Table 3. Confusion matrix for the CBIR experiment, using a kNN classifier with $k = 3$ and the Chebyshev distance.

Red	Yellow	Mixed	Retrieved for
30	5	16	Red
9	15	7	Yellow
24	6	54	Mixed

4 Discussion

Assessment of tissue composition provides crucial information to monitor the effects of treatment in patients with chronic ulcers. Quantitative measures can contribute to objective assessment of the healing process, and may be used for pattern recognition, CAD, and CBIR. Pattern recognition focuses on the classification of ulcers based on tissue composition to help enhance the diagnostic process and follow-up to treatment. CBIR is an approach to information retrieval and is more commonly used for medical decision-making based on previous and proven cases. If the results of a CBIR query bring images with one or more types of tissue composition, the clinician will be able to analyze them, determine which images are relevant, review the clinical reports associated with the retrieved images, and decide on the diagnostic classification of the image on hand. The clinician could also gain an understanding on why some of the retrieved images were classified into certain categories, either by an expert dermatologist or by the CBIR process. In this manner, the CBIR system could assist in arriving at a decision when the image on hand is at the boundaries between different categories. The concept of similarity is important because no two images may be expected to be identical, even when belonging to the same diagnostic category, and a perfect or exact match to a query image is unlikely. The use of vectors of quantitative parameters or features to index images facilitates the application of simple distance measures to select images that are most similar to the query sample, that is, to evaluate the similarity between images. Classification and CBIR applications may share the same set of image processing procedures, such as preprocessing, image segmentation, feature extraction, and categorization [11, 19, 21].

In a previous work based on the same images of manual segmentation of the ulcers by an experienced dermatologist [27], we obtained average AUC values of 0.820, and an average value of correctly classified instances divided by the total number of instances of 0.738. Results using automatic segmentation were observed to be poorer than those using manually segmented images. Therefore, our efforts to perform

automatic segmentation have yielded poorer results in terms of correct classification, which indicates that further improvements are needed. Nonetheless, our results of classification using a metaclassifier (average AUC value of 0.772) are encouraging.

Limitations of this work reside in the difficulty in applying the imaging protocol in a consistent manner. The images were not acquired in laboratory facilities, but in a clinical environment. In some cases, the patient's mobility affected positioning and imaging of the ulcers. Such difficulties also affected the distance and orientation of the camera, the illumination of the ulcer and the composition of the image. Procedures for color correction and normalization of images [39] need to be incorporated.

Another difficulty related to the current database is the variation of the size and position of the ulcers. It was observed that the clustering procedure tends to give better results when the ulcers are small, properly centered in the image, and without significant curvature. In such a situation, the number of Gaussians obtained by the clustering procedure was usually small, in the range of 3 to 5.

The segmentation results obtained in this pilot study have lower accuracy than desired, but are encouraging. Although the results are not very good in terms of the Jaccard coefficient, the small value obtained for the RMSE indicates that the estimation of tissue composition was not substantially affected by the limitations of the segmentation process. To improve the segmentation results, it would be desirable to include procedures for comparative analysis of an ulcer region with reference to the color characteristics of the surrounding normal skin of the patient. Further work is planned with a larger database of images, especially for the callous and necrotic categories of lesions, and also including longitudinal series of images of the same patients under treatment.

Clinical interpretation of images of dermatological ulcers is commonly based on visual analysis of the tissue composition as indicated by their color characteristics. This, however, is a qualitative approach that is affected by interobserver and intraobserver variability. Accurate estimation of the fractional composition of an ulcer in terms of tissue

types, such as granulation and fibrin, is nearly impossible via visual analysis. Quantitative evaluation of tissue composition provides key information for monitoring the response to treatment of patients with chronic ulcers and can assist in the evaluation of the healing process. In the present study, we have proposed the potential use of methods of digital image processing to achieve image segmentation focused on facilitating the characterization of the tissue composition of skin ulcers. We believe that objective analysis of color images of skin ulcers using the proposed methods can overcome some of the limitations of visual analysis and lead to the development of improved protocols for the treatment and monitoring of chronic dermatological lesions. Such advances, in turn, can assist in the design of optimized and personalized therapy for each patient.

References

[1] T. Chaira, A. K. Ray. *Fuzzy measures for color image retrieval.* Fuzzy Sets and Systems, 150:545–560, 2005.

[2] P. Welter, T. Deserno, B. Fischer, R. Gunther, C. Spreckelsen. *Towards case-based medical learning in radiological decision making using content-based image retrieval.* BMC Medical Informatics and Decision Making. 11(1):68:1–16, 2011.

[3] J. Z. Wang, J. Li, G. Wiederhold. *SIMPLIcity: Semantics-Sensitive Integrated Matching for Picture Libraries.* IEEE Transactions on Pattern Analysis and Machine Intelligence. 23(9):947–963, 2001.

[4] Q. Iqbal, J.K. Aggarwal. *CIRES: A system for content-based retrieval in digital image libraries.* International Conference on Control, Automation, Robotics and Vision (ICARCV), Singapore, 1:205-210, December 2–5, 2002.

[5] J. Ruiz-del-Solar, P. Navarrete. *FACERET: An interactive face retrieval system based on self-organizing maps.* In Image and Video

Retrieval - Lecture Notes in Computer Science, Springer, Berlin, Germany, 45–64, 2002.

[6] H. Müller, N. Michoux, D. Bandon, A. Geissbühler. *A review of content-based image retrieval systems in medical applications: clinical benefits and future directions.* International Journal of Medical Informatics, 73:1–23, 2004.

[7] H. Müller, A. Rosset, J. Vallée, F. Terrier, A. Geissbühler. *A reference data set for the evaluation of medical retrieval systems.* Computerized Medical Imaging and Graphics. 28:295–305, 2004.

[8] I. El-Naqa, Y. Yang, N. P. Galatsanos, R. M. Nishikawa, M. N. Wernick. *A similarity learning aprroach to content-based image retrieval: application to digital mammography.* IEEE Transactions on Medical Imaging. 23(10): 1233–1244, 2004.

[9] S. K. Kinoshita, P. M. Azevedo-Marques, R. R. Pereira Jr., J. A H. Rodrigues, R. M. Rangayyan. *Content-based retrieval of mammograms using visual features related to breast density patterns.* Journal of Digital Imaging. 20(2): 172–190, 2007.

[10] D. Tahmoush. *CBIR for mammograms using medical image similarity.* Medical Imaging 2010: Advanced PACS-based Imaging Informatics and Therapeutic Applications. Edited by B. J. Liu, W. W. Boonn. Proceedings of the SPIE. 7628(1):76280A 1–9, 2010.

[11] H. Alto, R.M. Rangayyan, J. E. L. Desautels. *Content-based retrieval and analysis of mammographic masses. Journal of Electronic Imaging.* 14(2):023016:1–17, 2005.

[12] C. R. Shyu, C. E. Brodley, A.C. Kak, A. Kosaka, A. M. Aisen, L. S. Broderick. *ASSERT: A physician-in-the-loop content-based image retrieval system for HRCT image databases.* Computer Vision and Image Understanding (Special Issue on Content-based Retrieval from Image Databases). 75(1/2): 111–132, 1999.

[13] M. C. Oliveira, W. Cirne, P. M. Azevedo-Marques. *Towards applying content-based image retrieval in the clinical routine*. Future Generation Computer Systems. 23:466–474, 2007.

[14] E. A. G. Dorileo, M. A. C. Frade, A. M. Roselino, R. M. Rangayyan, P. M. Azevedo-Marques. *Color image processing and content-based image retrieval techniques for the analysis of dermatological lesions*. In: Proc. 30th Annual International Conference of the IEEE Engineering in Medicine and Biology Society, Vancouver, BC, Canada. pages 1230–1233, August, 2008.

[15] L. Ballerini, X. Li, R. B. Fisher, J. Rees. *A query-by-example content-based image retrieval system of non-melanoma skin lesions*. In: Proc. International Conference on Medical Image Computing and Computer Assisted Intervention, London, UK, 5853:31–38, September, 2009.

[16] H. H. W. J. Bosman, N. Petkov, M. Jonkman. *Comparison of color representations for content-based image retrieval in dermatology*. Skin Research and Technology. 16:1–5, 2009.

[17] H. Wannous, S. Treuillet, Y. Lucas. *Robust tissue classification for reproducible wound assessment in telemedicine environments*. Journal of Electronic Imaging. 19(2):023002, 2010.

[18] J. Z. Wang. *Pathfinder: multiresolution region-based searching of pathology images using IRM*. In Proceedings of the AMIA Symposium, Los Angeles, CA, pp. 883887, November 4–8, 2000.

[19] P. M. Azevedo-Marques, R.M. Rangayyan. *Content-based Retrieval of Medical Images: Landmarking*, Indexing and, Relevance Feedback. Synthesis Lectures on Biomedical Enginering. Lecture #48, Morgan & Claypool, 2013.

[20] M. Antoine, O. R. Zaiane, A. Coman. *Application of data mining techniques for medical image classification*. Proceedings of the Second International Workshop on Multimedia Data Mining, MDM/KDD, 2001:94–101, San Francisco, CA, August 26, 2001.

[21] R. M. Rangayyan. *Biomedical Image Analysis*, CRC Press, Boca Raton, FL, 2005.

[22] T. M. Lehman, M. O. Güld, T. Deselaers, D. Keysers, H. Schubert, K. Spitzer, H. Ney, B. B. Wein. *Automatic categorization of medical images for content-based image retireval and data mining.* Computerized Medical Imaging and Graphics. 29:143–155, 2005.

[23] K. Doi. *Computer-aided diagnosis in medical images: Historical review, current status and future potential.* Computerized Medical Imaging and Graphics. 31:198–211, 2007.

[24] M. J. Callam, C. V. Ruckley, D. R. Harper, J. J. Dale. *Chronic ulceration of the leg: extent of the problem and provision of care.* British Medical Journal (Clinical Research Edition). 290(6485):1855–1856, 1985.

[25] I. Maglogiannis, S. Pavlopoulos, D. Koutsouris. *An integrated computer supported acquisition, and characterization system for pigmented skin lesions in dermatological images.* IEEE Transactions on Information Technology in Biomedicine. 9:86–98, March, 2005.

[26] H. Oduncu, A. Hoppe, M. Clarck, R. J. Williams, K. G. Harding. *Analysis of skin wound images using digital color image processing: a preliminary communication.* The International Journal of Lower Extremity Wounds. 3(3):151–156, 2004.

[27] S. M. Pereira, M. A. C. Frade, R. M. Rangayyan, P. M. Azevedo-Marques. *Classification of color images of dermatological ulcers.* IEEE Journal of Biomedical and Health Informatics. 17(1):136–142, 2013.

[28] E. A. G. Dorileo, M. A. C. Frade, R. M. Rangayyan, P. M. Azevedo-Marques. *Segmentation and analysis of the tissue composition of dermatological ulcers.* Proceedings of the Symposium of the IEEE Canadian Conference on Electrical and Computer Engineering, 1:1–4, Calgary, AB, Canada, May, 2010.

[29] H. Zheng, L. Bradley, D. Patterson, M. Galushka, J. Winder. *New protocol for leg ulcer tissue classification from colour images.* Proceedings of the 26th Annual International Conference of the IEEE Engineering in Medicine and Biology Society, San Francisco, CA, 1:13891392, September 1–4, 2004.

[30] A. S. Tarallo, A. Gonzaga, M. A. C. Frade. *Artificial neural networks applied to the segmentation and classification of digital images of cutaneous ulcers.* Proceedings of the IEEE 7th International Conference on Bioinformatics and Bioengineering, 1:1–1, Boston, MA, October 14-17, 2007.

[31] S. M. Pereira, M. A. C. Frade, R. M. Rangayyan, P. M. Azevedo-Marques. *Recuperao de imagens baseada em seu contedo: uma avaliao da performance de mtricas de distncia.* Proc. XXIII Congresso Brasileiro em Engenharia Biomdica XXIII CBEB, Porto de Galinhas, PE, Brasil, 1:1040-1044, October 2–5, 2012.

[32] M. E. Celebi, Y. A. Aslandogan. *Content-based image retrieval incorporating models of human perception.* Proceedings of the International Conference on Information Technology: International Conference on Coding and Computing, Las Vegas, NV, 2:241-245, April 5–7, 2004.

[33] M. M. Rahman, B. C. Desai, P. Bhattacharya. *Image retrieval-based decision support system for dermatoscopic images.* Proceedings of the 19th IEEE Symposium on Computer-based Medical Systems, Salt Lake City, UT, 285-290, 22–23 June, 2006.

[34] M. Celebi, Y. Aslandogan, P. Bergstresser, *Unsupervised border detection of skin lesion images.* Proceedings of the International Conference on Information Technology: International Conference on Coding and Computing, Las Vegas, NV, 2:123-128, April 4–6, 2005.

[35] P. Plassmann, T. Jones. *MAVIS: A non-invasive instrument to measure area and volume of wounds.* Medical Engineering and Physics, 20:332-338, 1998.

[36] P. M. Azevedo-Marques, S. M. Pereira, M. A. C. Frade, R. M. Rangayyan. *Segmentation of dermatological ulcers using clustering of color components*. In Proc. IEEE Canadian Conference on Electrical and Computer Engineering, Regina, SK, Canada, May 5-8, 2013.

[37] P. Dempster, N. M Laird, D. B. Rubin. *Maximum likelihood from incomplete data via the EM algorithm*. Journal of the Royal Statistical Society. 39(1):1–38, 1977.

[38] F. Pernkopf, D. Bouchaffra. *Genetic-based EM algorithm for learning Gaussian mixture models*. IEEE Transactions on Pattern Analysis and Machine Intelligence. 39(8):1344–1348, 2005.

[39] R. M. Rangayyan, B. Acha, C. Serrano, *Color Image Processing with Biomedical Applications*. SPIE Press, Bellingham, WA, 2011.

[40] A. Ford, A. Roberts. *Color Space Conversions*. Technical report. Westminster University, London, 1998.

[41] S. R. Garner. *WEKA: The Waikato Environment for Knowledge Analysis*. In Proc. of the New Zealand Computer Science Research Students' Conference, Hamilton, New Zealand, 1:57-64, April 18–21, 1995.

[42] R. C. Gonzalez, R. E. Woods. *Digital Image Processing*, 221–248, Addison-Wesley, New York, NY, 1993.

[43] R. M. Haralick, K. Shanmugam, I. Dinstein. *Textural features for image classification*. IEEE Transactions on Systems, Man, and Cybernetics. 3:610–621, 1973.

[44] R. W. Conners, C. A. Harlow. *A theoretical comparison of texture algorithms*. IEEE Transactions on Pattern Analysis and Machine Intelligence. 2:204–222, 1980.

[45] V. Arvis, C. Debain, M. Berducat, A. Benassi. *Generalization of the cooccurrence matrix for colour images: application to colour*

texture classification. Image Analysis and Stereology, 23(1):63–72, 2011.

[46] S. Le-Cessiet, J.C Van-Howelingen. *Ridge estimators in logistic regression*. Applied Statistics. 41(1):191–201, 1992.

Lucas C. Pereyra, Sílvio M. Pereira, Juliana P. Souza, Marco A. C. Frade, Rangaraj M. Rangayyan, Paulo M. Azevedo-Marques

Received May 19, 2014

Lucas C. Pereyra
Ribeirão Preto Medical School, University of São Paulo
Av. dos Bandeirantes 3900, Monte Alegre, 14049-900, Ribeirão Preto - SP, Brazil
E–mail: *lucascalabrez@gmail.com*

Sílvio M. Pereira
Bioengineering Interunits Graduate Course, University of São Paulo
São Carlos - SP, Brazil
E–mail: *silviomoreto@usp.br*

Juliana P. Souza
Ribeirão Preto Medical School, University of São Paulo
Av. dos Bandeirantes 3900, Monte Alegre, 14049-900, Ribeirão Preto - SP, Brazil
E–mail: *jupsouza@usp.br*

Marco A. C. Frade
Ribeirão Preto Medical School, University of São Paulo
Av. dos Bandeirantes 3900, Monte Alegre, 14049-900, Ribeirão Preto - SP, Brazil
E–mail: *mandrey@fmrp.usp.br*

Rangaraj M. Rangayyan
Department of Electrical and Computer Engineering, Schulich School of Engineering, University of Calgary, Calgary, Alberta, T2N 1N4, Canada
E–mail: *ranga@ucalgary.ca*

Paulo M. Azevedo-Marques
Ribeirão Preto Medical School, University of São Paulo
Av. dos Bandeirantes 3900, Monte Alegre, 14049-900, Ribeirão Preto - SP, Brazil
E–mail: *pmarques@fmrp.usp.br*